Phys Chem Minerals (2003) 30: 12–19
DOI 10.1007/s00269-002-0285-z

ORIGINAL PAPER

R. Stalder · H. Skogby

Hydrogen diffusion in natural and synthetic orthopyroxene

Received: 22 February 2002 / Accepted: 18 October 2002

Abstract Hydrogen diffusion coefficients in natural orthopyroxenes and synthetic enstatite were determined by dehydration and hydration experiments at 700 and 900 °C. In natural Opx (approximately $En_{90}Fs_{10}$) small but significant differences in diffusivities along the three crystallographic axes were observed, [001] being the fastest direction, followed by [100] and [010]. Hydrogen diffusion in pure enstatite proved to be about 2 orders of magnitude slower and isotropic. The activation energy for hydrogen diffusion in pure enstatite was determined to be −295 (±55) kJmol^{-1}, and −213 (±47) kJmol^{-1} for orthopyroxene from Kilbourne Hole. Long-term hydration experiments did not lead to saturation in hydrogen. Instead, after an initial increase in hydrogen concentration, a slow but continuing decrease could be observed in all cases. It is suggested that the investigated samples lose their ability to store hydrogen even when heated in a hydrogen atmosphere. This loss in storage ability can itself be described by a diffusion equation, its diffusion coefficients being more than 1 order of magnitude slower than the diffusion of hydrogen.

Keywords Enstatite · Hydrogen diffusion · Infrared spectroscopy

Introduction

Although orthopyroxene is nominally anhydrous, it is able to dissolve traces of OH as point defects (Bell and Rossman 1992) and may be a major host for water in the mantle. However, although the OH concentration of natural orthopyroxenes varies as a function of their geological setting (Skogby et al. 1990), it has been argued that samples from xenoliths from the upper mantle might have undergone a partial water loss during ascent (Ingrin and Skogby 2000), as has been demonstrated by diffusion experiments on single crystals of other mantle minerals (olivine: Mackwell and Kohlstedt 1990; clinopyroxene: Ingrin et al. 1995; Hercule and Ingrin 1999; Carpenter et al. 2000). So far, only few diffusion data on natural orthopyroxene have been determined (Carpenter and Mackwell 1999), whereas no diffusion data for pure enstatite have as yet been reported.

Here, we report hydrogen diffusion coefficients along the crystallographic axes determined by dehydration experiments on pure synthetic enstatites between 700 and 900 °C. The obtained data are compared with diffusion coefficients determined by hydration and dehydration experiments on natural orthopyroxenes from spinel lherzolite xenoliths from Kilbourne Hole, New Mexico, and Hoher Hagen, Germany. Another task of the hydration experiments was to investigate the amount of hydrogen that can be incorporated at 1 atm ambient pressure. Results from this kind of experiment may give an answer to the question of how much hydrogen was lost during ascent from the upper mantle.

R. Stalder (✉) · H. Skogby
Naturhistoriska riksmuseet, Sektionen för mineralogi,
Box 50007, 10405 Stockholm, Sweden
e-mail: rstalde@gwdg.de
Tel.: +49-551-393886
Fax: +49-551-393863

Present address: R. Stalder
Abteilung Experimentelle & Angewandte Mineralogie,
Geowissenschaftliches Zentrum der Universität Göttingen,
Goldschmidtstraße 1,37077 Göttingen, Germany

Experimental

Single crystals of pure enstatite were synthesized from specpure oxides at 25 kbar under H_2O-saturated conditions (Stalder 2002). Large crystals (up to several mm^3) were selected by handpicking, embedded in a thermoplastic resin and oriented according to the crystallographic axes using a microscope with polarized transmitted light. For orientation, the optical properties (birefringence, conoscopic interference figure) were used. Thereafter, all crystals were ground and polished on both sides and the thickness of each prepared crystal was determined mechanically. Natural orthopyroxenes from spinel lherzolite xenoliths from Kilbourne Hole (New Mexico) and Hoher Hagen (Germany) were prepared in the same way. In contrast to the synthetic samples, which exhibit well-developed crystal faces and were elongated along the crystallographic *c* axis, natural samples often did not show unambiguous

morphology. Preparation was therefore carried out in several steps, until the correct orientation had been reached. Orthopyroxene crystals from Hoher Hagen were very fine-grained and partly weathered on the surface; therefore only very few and small preparable crystals could be separated from the source rock. Preparation parallel to (001) turned out be particularly difficult, as the preferred cleavage parallel (110) split the crystal into many fragments as soon as a thickness became smaller than 350 μm. Therefore, the preparation of a synthetic enstatite parallel (001) was not successful and was abandoned after several unsuccessful trials. The prepared crystals from Kilbourne Hole and En7 (synthetic) measured approximately 1–1.5 mm in both directions parallel to the polished surface, and were considerably thinner perpendicular to it (Table 1). An exception is sample no. 15 with about 0.5 mm length and width. The crystal from Hoher Hagen was about 400×300 μm.

For the kinetic studies, samples were stepwise dehydrated in air or hydrated in an H_2 atmosphere in a horizontal furnace with a constant gas flow (Table 1). Sample 17 was dehydrated in two steps and then partly rehydrated. The temperature was controlled with a Pt_{100}–$Pt_{90}Rh_{10}$ thermocouple located exactly above the samples. The temperature is estimated to be correct within ±2 °C.

Polarized IR spectra before and after each hydration/dehydration run were recorded with a Bruker IFS 48 spectrometer at the University of Linköping (in a later stage of the project a Perkin-Elmer Spectrum 2000 at the Kungliga Tekniska Högskolan in Stockholm was used). For each analysis 64–100 scans within the range $1000 - 5000\,cm^{-1}$ were acquired in absorbance mode. Samples were measured in the centre in both crystallographic directions using circular apertures with a diameter between 100 and 300 μm. In some cases, profiles across the whole section were recorded, where apertures between 40 and 70 μm were used. Raw data spectra were processed with a PeakFit program (Jandel Scientific). Integrated intensities of the absorption bands were determined by fitting the background-corrected spectra to Gaussian area functions. Peak intensities were then converted into H_2O concentrations using the calibration of Libowitzky and Rossman (1997). This calibration was favoured against the calibration of Bell et al. (1995), as the contribution of each peak to the total concentration is distinguished. Since not all peak intensities change in the same way when samples are dehydrated or hydrated (Fig. 1), untreated and treated samples can be compared more reliably.

Several individual grains from the synthetic enstatite and from orthopyroxene from Kilbourne Hole, and the prepared crystal from Hoher Hagen, were embedded for electron microprobe analysis and were analyzed with a Cameca SX50 electron microprobe at the University of Uppsala using an acceleration voltage of 20 kV and at a sample current of 15 nA (Table 2). In addition, orthopyroxenes from Kilbourne Hole were analyzed by Mößbauer spectroscopy at 298 and 77 K; 96.5% of all iron was ferrous (Fe^{2+}) and 3.5% ferric (Fe^{3+}).

Results

Results of the stepwise-treated samples are summarized in Table 3. Spectra of a typical dehydration series are shown in Fig. 1. As the thickness of the samples perpendicular to the polished surfaces was much smaller than parallel to them, and diffusion coefficients were expected to be not strongly anisotropic, diffusion coefficients were calculated using the solution of Fick's second law for one-dimensional diffusion in a solid with a homogeneous initial concentration bounded by two parallel planes (Carslaw and Jaeger 1959; Ingrin et al. 1995). For dehydration, the average OH concentration across the crystal plate follows the equation

$$\frac{c_{av}}{c_0} = \frac{8}{\pi^2} \cdot \sum_{n=0}^{\infty} \frac{1}{(2n+1)^2} \cdot e^{\left(\frac{-Dt(2n+1)^2 \cdot \pi^2}{4L^2}\right)} \quad , \qquad (1)$$

c_{av} being the average concentration across the whole thickness of the crystal plate, c_0 the initial concentration of the diffusing species, D the diffusion coefficient, t the time and $2L$ the thickness of the sample. When calculating diffusion coefficients, it has been assumed that, due to the geometry of the specimens, diffusion occurred predominantly along one direction. When the first results were obtained, Eq. (1) was also applied to test whether diffusion could have taken place mainly in one of the other directions (i.e., the long dimensions of the specimen) due to anisotropy. Hypothetical diffusion coefficients obtained in this way set an upper limit for diffusion in the respective direction, and were significantly faster than those given in Table 3, suggesting that the influence from the other two directions can be neglected. Furthermore, the determined diffusion coefficients are not dependent on the thickness of the samples. Samples 16 and 20 furnish basically the same result for $D_{[010]}$, even if 16 was about four times thicker than 20 (both have the same dimensions along [100] and [001]). Only if calculation of the diffusion coefficient for no. 16 had resulted in a significantly faster diffusion, diffusion along the fastest direction [001] would have had to be taken into account. The simplification of

Table 1 Details of dehydration and hydration experiments. All times are increment times

Sample no.	Sample	Orientation	Thickness (μm)	T (°C)	Atmosphere	t_1 (h)	t_2 (h)	t_3 (h)
13	KBH1[a]	∥ (100)	185	700	H_2	24	96	336
15	KBH1	∥ (010)	215	700	H_2	24	96	336
16	KBH1	∥ (010)	288	700	Air	24	168	192
17	KBH1	∥ (100)	127	700	Air/Air/ H_2	24	20	336
18	HH[b]	∥ (010)	40	700	H_2	24	96	
20	KBH1	∥ (010)	73	700	Air	2	2	6
23	KBH1	∥ (100)	70	700	Air	2	1	
25	KBH1	∥ (001)	340	700	Air	18	18	18
26	En7 syn.	∥ (010)	120	700	Air	4	148	480
28	En7 syn.	∥ (100)	80	700	Air	1	148	480
34	En7 syn.	∥ (010)	198	900	Air	2	6	
35	En7 syn.	∥ (100)	100	900	Air	6		

[a] KBH1 = Kilbourne Hole, New Mexico
[b] HH = Hoher Hagen, Germany

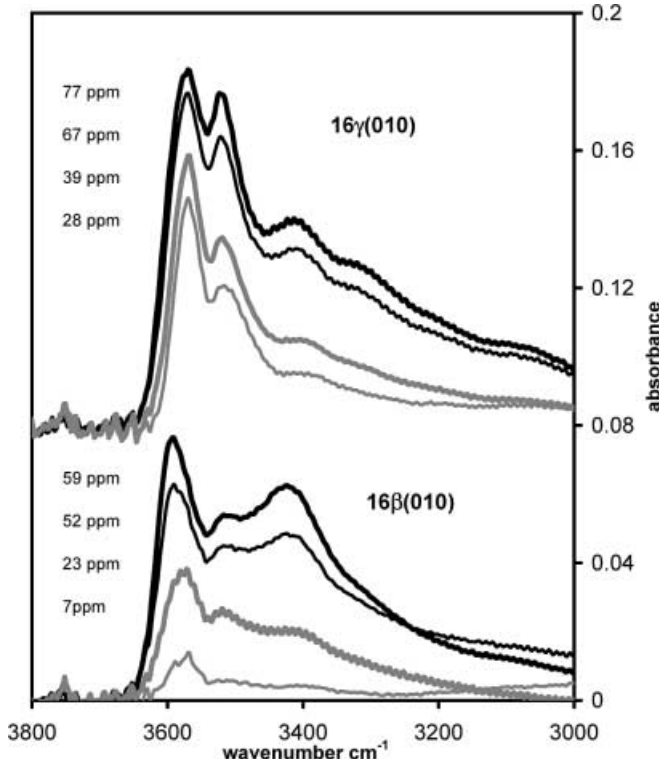

Fig. 1 IR spectra of sample 16 from KBH1 from both directions on the (010) plane. *Different curves* show absorbances after each dehydration step; *thick black* initial absorbance; *thin black* after 24 h; *thick grey* after 192 h; *thin grey* after 384 h. Corresponding concentrations (wt H_2O) are given at the left. Spectra are not normalized to the sample thickness (288 μm)

unidirectional diffusion is suitable for nearly all samples described here. The only exception is sample 15, measuring 215, 500 and 500 μm along [010], [100] and [001], respectively. Using the diffusion coefficient determined on the other samples, according to Eq. (1), the strongest H flux occurs along [001], but significant diffusion occurs in all directions. Therefore the resulting diffusion coefficient is about 0.3 log units higher than for diffusion along [001] alone.

Table 2 Microprobe analyses of samples used in this study

Sample	Kilbourne Hole, New Mexico	Hoher Hagen, Germany	En7 synthetic
SiO_2	53.93 ± 0.59	55.02 ± 0.56	59.32 ± 0.56
MgO	32.80 ± 0.28	34.54 ± 0.70	40.75 ± 0.36
Al_2O_3	4.68 ± 0.08	3.23 ± 0.31	
FeO	6.06 ± 0.04	5.64 ± 0.09	
TiO_2	0.10 ± 0.03	0.09 ± 0.02	
Cr_2O_3	0.46 ± 0.03	0.30 ± 0.04	
CaO	0.86 ± 0.03	0.68 ± 0.46	
MnO	0.12 ± 0.03	0.14 ± 0.02	
Na_2O	0.11 ± 0.04	0.08 ± 0.06	

At a given time (t = constant) the concentration as a function of the location x along a profile averaged across the whole thickness of the plate can be expressed as:

$$\frac{c_{av}}{c_0} = \frac{4}{\pi} \cdot \sum_{\pi=0}^{\infty} \frac{(-1)^n}{(2n+1)} \cdot e^{\left(\frac{-Dt(2n+1)^2 \cdot \pi^2}{4L^2}\right)} \cos\left(\frac{(2n+1)\pi x}{2L}\right) . \quad (2)$$

Diffusion coefficients calculated in either of these ways are presented in Table 3; the results from the dehydration experiment of the natural orthopyroxenes with the calculated concentration curve are given in Fig. 2a–e. A profile along [100] measured on the (010) surface of a crystal from KBH1 is given in Fig. 3. The profile shows a clear plateau. Inside this plateau diffusion can be considered as occurring nearly only along [010]. The diffusion was considered as two independent processes, diffusion along [010], decreasing the concentration of the plateau, and along [100], evolving the profile. The calculated diffusion coefficient along [100] for the measured profile matches the value determined by dehydration on the thin samples 17 and 23. Results from dehydration runs of the synthetic pure enstatites are shown in Fig. 4a–d. Spectra of samples dehydrated at 900 °C showed much broader peaks than dehydrated samples at

Table 3 Results of IR spectroscopy. Only the two components parallel to the polished surface were measured; absorbances are expressed as H_2O concentrations in ppm

	c_0	c_1	c_2	c_3	$-\log D$ [100]	$-\log D$ [010]	$-\log D$ [001]	$-\log D_v$
Sample No. Dehydration experiments								
16	133	119	62	35	13.7[a]	14.2		
17	131	43	29		13.8			
20	124	99	72	63		14.1		
23	149	70	58		13.4			
25	160	79	62	51			13.2	
26	198	204	158	118		15.7		
28	244	247	204	86	15.8			
34	182	132	66			13.0		
35	256	37			13.1			
Hydration experiments								
13	122	169	188	132	13.5			15.1
15	125	151	169	141			12.9[b]	14.4
17			29	111	13.8			15.1
18	37	127	53			14.2		15.4

[a] Derived from diffusion profile
[b] Also contribution from [100] and [010]

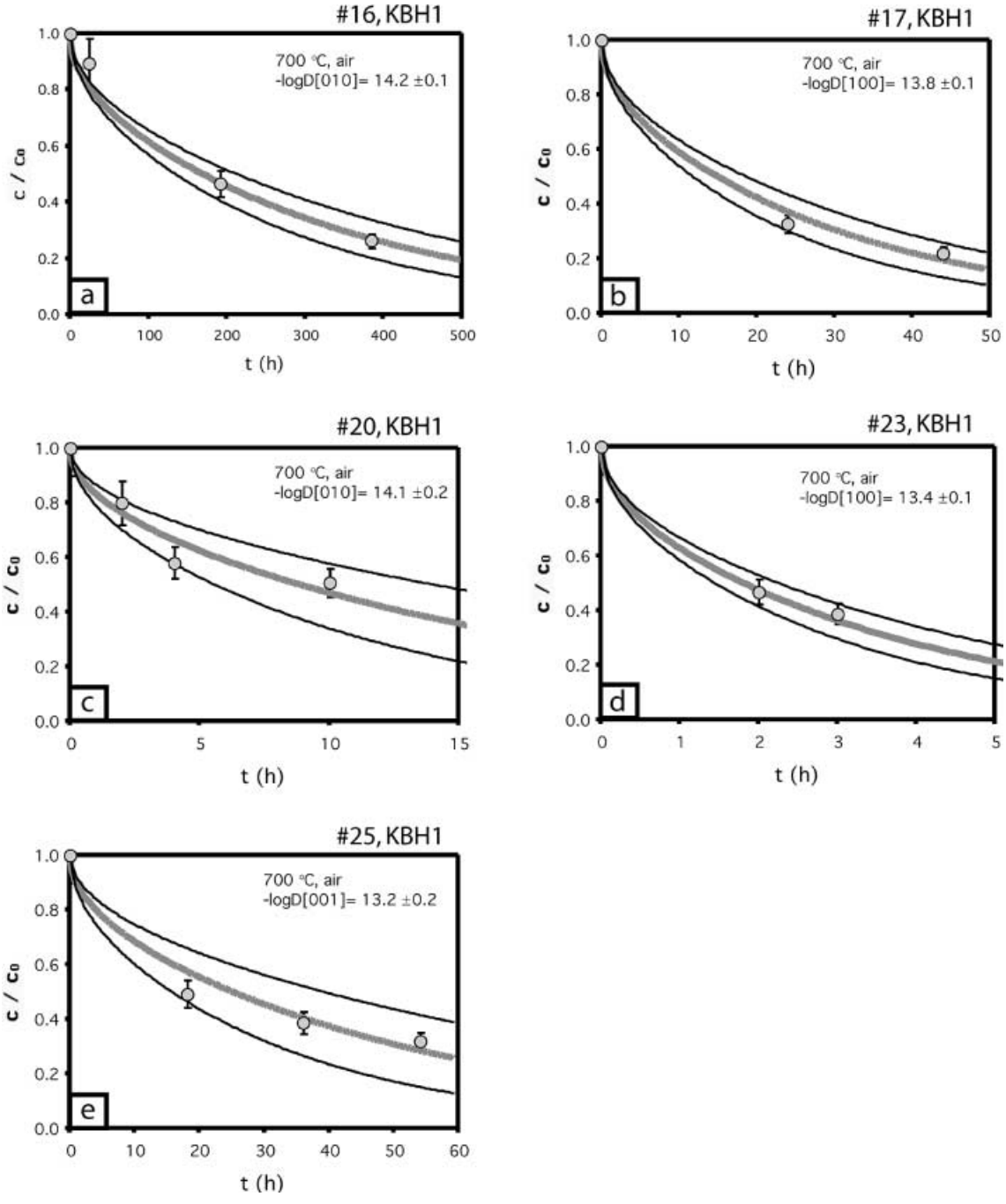

Fig. 2a–e Hydrogen diffusion coefficients determined by dehydration experiments on samples from KBH1. *Thick grey curves* correspond to the diffusion coefficient given in the *upper right of each diagram* and *black curves* correspond to the upper and lower limit of the given error. Diffusion along [010] (**a**,**c**) is about 1 order of magnitude slower than along [001] (**e**), whereas [100] has values in between (**b**,**d**)

700 °C. Furthermore, two additional broad peaks occurred between 2700 and 3000 cm^{-1}. The resulting diffusion coefficients were fitted to an Arrhenius equation

$$D = D_0 \cdot e^{\left(\frac{-E_a}{RT}\right)} \quad , \tag{3}$$

where D_0 is the diffusivity at infinite temperature and E_a is the activation energy. The results are shown in an Arrhenius plot (Fig. 5). The activation energy of hydrogen diffusion along [100] and [010] can be calculated as -295 ± 55 kJ mol^{-1} in pure enstatite; D_0 calculates as 1.37 m^2s^{-1}. In order to establish an activation energy also for the natural orthopyroxene, a diffusion coefficient was calculated from a hydrogen extraction experiment at 1000 °C reported by Bell et al. (1995), also performed on KBH1 orthopyroxene, which leads to a $\log D[001] = -10.5$. The resulting diffusion parameter can then be given as $E_a = -213 \pm 47$ kJ mol^{-1} and $D_0 = 0.018$ m^2s^{-1}.

The interpretation of the hydration runs turned out to be more complicated. Unlike hydration experiments

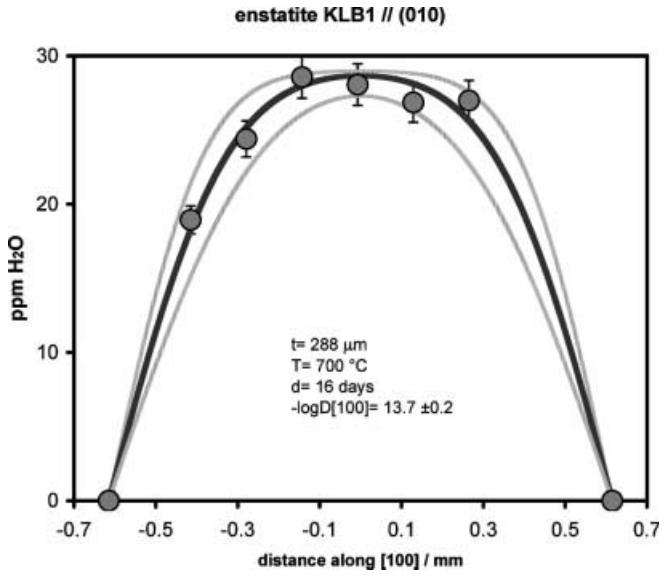

Fig. 3 Diffusion profile along [100] on the (010) plane. The diameter of the crystal was about 1.25 mm. Only the γ-component was measured; intensities are converted to H_2O concentrations according to the calibration of Libowitzky and Rossman (1997)

on diopside (Hercule and Ingrin 1999), the concentration did not reach a stable saturation value. Instead, in all hydration runs a slow decrease in OH concentration could be observed after an initial increase. However, if the saturation level was not considered as a fixed value, but as a value decreasing following the diffusion law, the shape of the spectra could be modelled with the equation

$$\frac{c_{\mathrm{av}}}{c_0} = \left\{ \left[1 - \frac{8}{\pi^2} \cdot \sum_{n=0}^{\infty} \frac{1}{(2n+1)^2} \cdot e^{\left(\frac{-D_1 t (2n+1)^2 \cdot \pi^2}{4L^2}\right)} \right] \cdot \left(1 - \frac{c_n}{c_{\mathrm{sat}}} \right) + \frac{c_n}{c_{\mathrm{sat}}} \right\} + \left\{ \left[\frac{8}{\pi^2} \cdot \sum_{n=0}^{\infty} \frac{1}{(2n+1)^2} \cdot e^{\left(\frac{-D_2 t (2n+1)^2 \cdot \pi^2}{4L^2}\right)} \right] - 1 \right\}, \quad (4)$$

which is essentially a combination of two diffusion processes described by Eq. (1). C_{sat} is the hypothetic saturation concentration, D_1 is the diffusion coefficient of the diffusing species (in this case hydrogen, which diffuses into the crystal) and D_2 represents a slower diffusion process of another species out of the crystal. The physical meaning of this second diffusion process will be discussed later. The first part of Eq. (4) gives the increasing amount of hydrogen and the second part the decreasing part of the hydrogen in the crystal. The term c_n/c_{sat} is needed to match the initial concentration. A graphical illustration is given in Fig. 6. Calculated diffusion coefficients of the hydration runs are shown Fig. 7a–d. In contrast to the dehydration experiments, the observed concentrations within one series cannot be fitted unequivocally unless the diffusion coefficient for hydrogen determined in the dehydration experiments is inserted in Eq. (4). Otherwise, based on the present data, several different combinations of the three unknowns (i.e., hypothetical saturation level and both diffusion coefficients) lead to a curve that is in accord with the observations (Fig. 7c–d).

Discussion

Comparison with other studies

Diffusion coefficients for hydrogen in orthopyroxenes from KBH1 are very similar to those of orthopyroxene from San Carlos, Arizona (Carpenter and Mackwell 1999), with an FeO content of 5.3 wt% and an Al_2O_3 content of 2.4 wt%. Similar to the findings of our study, San Carlos orthopyroxenes showed anisotropic diffusion behaviour, [001] being the most rapid diffusion direction. From their Arrhenius equation the value for $-\log D$[001] at 700 °C can be calculated as 13.4, which compares very well with the value 13.2 determined for KBH1 in the present study. Hydrogen diffusion coefficients for natural orthopyroxenes are in the same order of magnitude as diffusion coefficients determined by extraction–incorporation experiments on diopside ($-\log D = 13.5$ at 700 °C, Ingrin et al. 1995), which later, when H–D exchange experiments were carried out (Hercule and Ingrin 1999), turned out to most likely represent electron-hole mobility. Self-diffusion coefficients were 1 to 2 orders of magnitude higher, and revealed, in contrast to electron-hole mobility, a clearly developed anisotropic behaviour, diffusion along [010] being the slowest. From these findings, Hercule and Ingrin (1999) concluded that the mobility of electron holes, rather than the mobility of hydrogen itself, can be considered as the rate-limiting step during hydrogen diffusion in diopside. Furthermore, the mobility of electron holes was shown to be dependent on the Fe content of the sample, and a threshold of 6 to 8 at% Fe/(Fe + Mg) was proposed, above which the mobility of the electron holes became fast enough for hydrogen self-diffusion to become the rate-limiting process.

In the present study no deuteriation experiments were carried out, and therefore it cannot be unequivocally answered whether the determined values represent hydrogen self-diffusion coefficients or are controlled by electron hole mobility. On the one hand, the significant anisotropy in diffusion behaviour determined on orthopyroxenes from KBH1 is in analogy to hydrogen self-diffusion in diopside, and the Fe content of samples from KBH1 is well above the proposed threshold value for diopside. On the other hand, the determined diffusion coefficients are 2 orders of magnitude slower than self-diffusion coefficients of hydrogen in diopside (Hercule and Ingrin 1999) and hydrogen diffusion in olivine (Mackwell and Kohlstedt 1990), and slightly slower than in garnet (Wang et al. 1996). In other words, orthopyroxenes and clinopy-

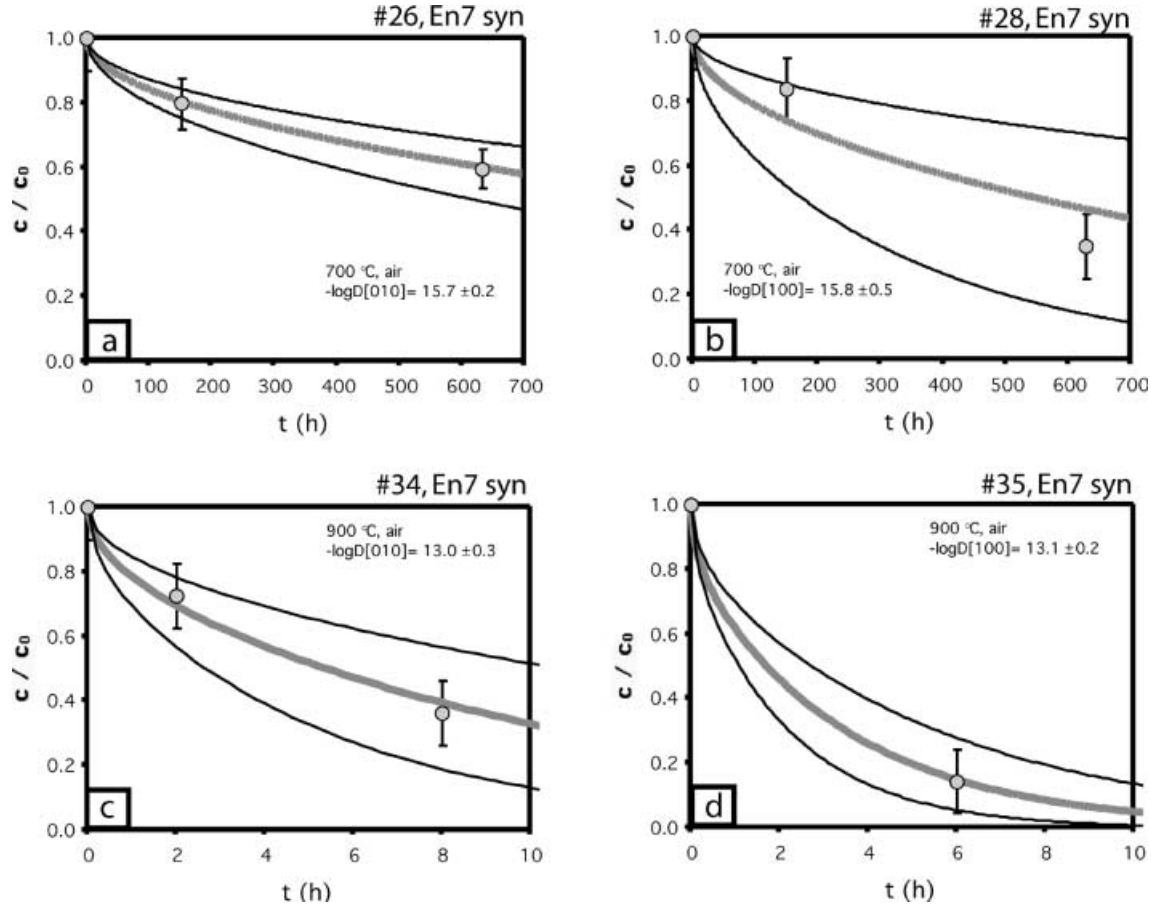

Fig. 4a–d Hydrogen diffusion coefficients determined by dehydration experiments on samples from En7 (synthetic). *Thick grey curves* correspond to the diffusion coefficient given in each diagram and *black curves* correspond to the upper and lower limit of the given error

roxenes from upper-mantle samples are expected to show the least hydrogen loss during ascent. If it is assumed that during ascent equilibrium within a mantle xenolith is attained quickly, it is the amount of hydrogen in the pyroxenes that controls the hydrogen

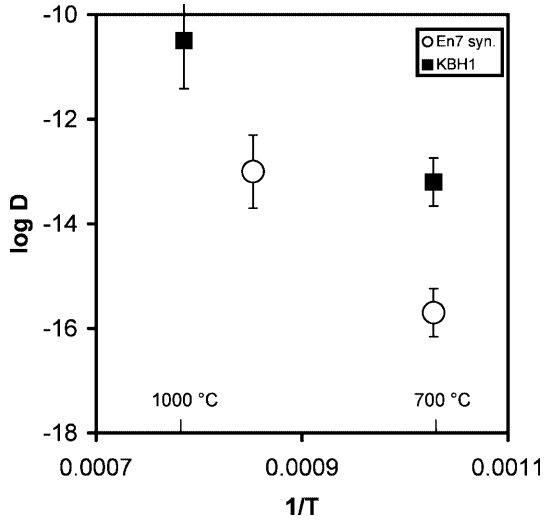

Fig. 5 Arrhenius plot showing H diffusion in synthetic enstatite along [010] and in orthopyroxene from KBH1 along [001]. The value for 1000 °C from KBH1 is calculated from results of Bell et al. (1995). From the slope of the graph E_a can be calculated as -295 ± 55 kJ mol^{-1} and -213 ± 47 kJ mol^{-1} for pure enstatite and the natural orthopyroxene, respectively

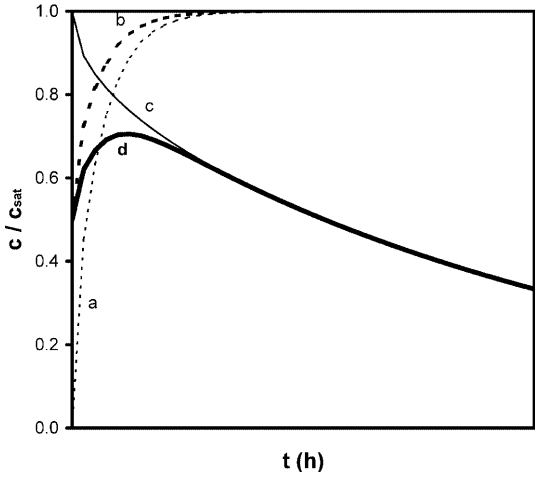

Fig. 6 Graphical illustration of Eq. (4). *a* Saturation curve beginning from $c_0 = 0$; *b* saturation curve beginning from $c_0 > 0$; *c* dehydration curve; $d = b + c - 1$. The diffusion coefficient used for curve *c* is much smaller than for curve *b*

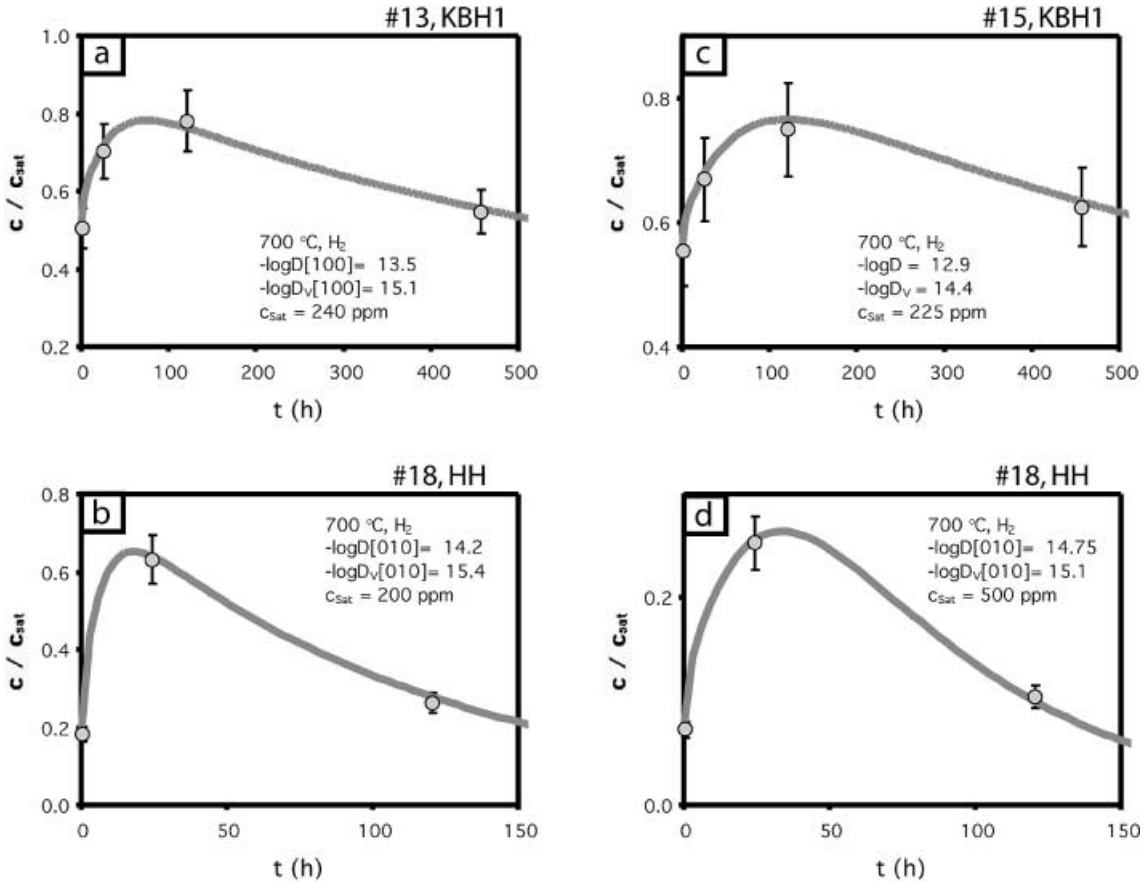

Fig. 7a–d OH concentration evolution observed in hydration experiments on samples from KBH1 and HH. *Thick grey curves* correspond to calculations performed according Eq. (4), the applied diffusion coefficients being given in each diagram. C_{sat} refers to the saturation level calculated for two of the three concentration components measured on the respective crystal. The saturation concentration for the whole crystal ($\alpha + \beta + \gamma$) is about 50% higher. *LogD* refers to hydrogen diffusion; $logD_V$ refers to diffusion of some sort of defect, describing the ability to store hydrogen; C_{sat} gives the hypothetical saturation level. Diffusion coefficients given for sample 15 are calculated for the [001] direction. However, they do not represent unidirectional diffusion as, due to the geometry of the sample, a significant contribution from [010] and [100] occurred. If the flux in the other direction is estimated to be as big as along [001], D[001] is 0.3 log units lower (i.e., $-\log D[001] = 13.2$

fugacity in the whole xenolith during the eruption process at low surrounding pressure.

Hydration experiments

The reason for the loss of ability to store H_2O observed in the long-term hydration experiments, and the physical meaning of the postulated additional diffusion coefficient for this second process, remain unsure. For hydrogen diffusion in olivine Mackwell and Kohlstedt (1990) suggested that the hydrogen flux is coupled with a flux of electron holes. On the other hand, electron mobility can be the rate-limiting step (Hercule and Ingrin 1999). The second diffusion process suggested from the hydration experiments reported here is about 1.5 log units slower than hydrogen diffusion, which corresponds to the difference between hydrogen self-diffusion and electron-hole mobility in diopside (Ingrin et al. 1995; Hercule and Ingrin 1999). On the other hand, this second process seems – in contrast to electron-hole mobility in diopside – to be anisotropic also. Diffusion coefficients determined for pure enstatite could be regarded as a lower limit for electron-hole mobility, as no charge compensation is available. The second diffusion process observed upon hydration is significantly faster than the diffusion coefficients determined on pure enstatite in this study. This may be due to differences in chemical composition. An alternative explanation may be some sorts of natural dislocations or point defects in the orthopyroxene lattice, which anneal during thermal treatment.

Diffusion and hydrogen incorporation at different temperature

The activation energy for hydrogen diffusion in orthopyroxene from KBH1 determined in this study agrees with activation energies determined on some other natural orthopyroxenes from previous experiments (161 kJ mol^{-1} for a Fe-poor sample from Sri Lanka, and 195 kJ mol^{-1} for an orthopyroxene from San Carlos; Carpenter and Mackwell 1999), but is somewhat higher

than for diopside (126–149 kJmol^{-1}, Hercule and Ingrin 1999; 153–181 kJmol^{-1}, Carpenter et al. 2000). Activation energies for natural orthopyroxene seem to define a narrow field similar to diopside. The only exception hitherto reported is an orthopyroxene from Sri Lanka (Carpenter and Mackwell 1999) containing 8.5 wt% FeO and 3.6 wt% Al_2O_3 with an activation energy of 326 kJ mol^{-1}, close to the value determined for pure enstatite in this study. No obvious dependence of the hydrogen diffusion activation energy on the chemical composition could be established.

The drastic changes in the peak shape of all IR spectra observed in dehydration runs at 900 °C on pure, synthetic enstatite reflect a change in the local environment of the incorporated hydrogen. The peak broadening could be explained by a more statistical (i.e., disordered) hydrogen distribution occurring at higher temperature.

Petrological application

Before being treated in H_2 atmosphere, samples from KBH1 contained about 200 ppm H_2O (values in Table 3 are summed from two of the three components α, β and γ), comparable to the 186 ppm determined by Bell et al. (1995). The hydrogen uptake during heating in an H_2 atmosphere can be considered as a redox reaction

$$Fe^{3+} + O^{2-} + \tfrac{1}{2}H_2(g) = Fe^{2+} + OH^- \quad , \qquad (5)$$

as earlier proposed for amphiboles (Clowe et al. 1988; Dyar et al. 1993), diopside (Ingrin et al. 1989; Skogby and Rossman 1989; Skogby 1994) and olivine (Mackwell and Kohlstedt 1990). The hydrogen uptake may reflect an earlier hydrogen loss during ascent from the upper mantle. In the case of untreated KBH1 0.17 wt% Fe^{3+} was present, which would correspond to an increase in H_2O by approximately 270 ppm if reaction (5) was complete, leading to a total water content of 470 ppm. Results from high-pressure experiments suggest H_2O solubilities in pure enstatite within the spinel lherzolite stability field (15–25 kbar) of 200–300 ppm (Rauch and Keppler 2002; Stalder 2002). A sample containing 1.5 wt% Al_2O_3 dissolved up to a factor of 2 more H_2O (Rauch and Keppler 1998). On the other hand, saturation levels modelled in Eq. (4) furnish a slightly smaller number (225 and 240 ppm, respectively). As in that calculation only two of the three dipole components are taken into account, the saturation concentration in H_2O can be estimated to be approximately 50% higher, i.e., 350 ppm. In summary, under mantle conditions, orthopyroxene from KBH1 may have contained between 350 and 470 ppm H_2O. Interestingly, the samples from Hoher Hagen initially contained much less H_2O (about 50 ppm) than samples from KBH1; however, after hydration, more similar H_2O contents were observed. In addition, the modelled saturation level of samples from both localities is very similar. For some reason, orthopyroxenes from HH suffered a much stronger H_2O loss than those from KBH1. The reason may be found in the different ascent history of magmas of the two localities.

Acknowledgements This project was financed by the EU research training network HYDROSPEC (Contract. no. HPRN-CT-2000–00056) and the Swedish Research Council. Bo Liedberg (Institutionen för Fysik och Mätteknik, University of Linköping) and Mats Johansson (Dept. of Polymer Technology, Kungliga Tekniska Högskolan, Stockholm) kindly provided access to IR spectroscopy, and Hans Harryson (University of Uppsala) is thanked for helping with the microprobe analyses. David Bell is thanked for providing starting material from KBH1.

References

Bell DR, Rossman GR (1992) Water in the Earth's mantle: the role of nominally anhydrous minerals. Science 255: 1391–1397

Bell DR, Ihinger PD, Rossman GR (1995) Quantitative analysis of trace OH in garnet and pyroxenes. Am Mineral 80: 465–474

Carpenter SJ, Mackwell SJ (1999) Hydrogen diffusion in enstatite. Bayrisches Forschungsinstitut für experimentelle Geochemie und Geophysik, annual report, 70 (http://www.bgi.uni-bayreuth.de)

Carpenter S, Mackwell S, Dyar D (2000) Hydrogen in diopside: diffusion profiles. Am Mineral 85: 480–487

Carslaw HS, Jaeger JC (1959) Conduction of heat in solids. Clarendon, Oxford, UK, 510 pp

Clowe CA, Popp RK, Fritz SJ (1988) Experimental investigation of the effect of oxygen fugacity on ferric ferrous ratios and unit cell parameters of four natural clinoamphiboles. Am Mineral 73: 487–499

Dyar MD, Mackwell SJ, McGuire AV, Cross LR, Robertson JD (1993) Crystal chemistry of Fe^{3+} and H^+ in mantle kaersutite: implications for mantle metasomatism. Am Mineral 78: 968–979

Hercule S, Ingrin J (1999) Hydrogen in diopside: diffusion, kinetics of extraction–incorporation, and solubility. Am Mineral 84: 1577–1587

Ingrin J, Skogby H (2000) Hydrogen in nominally anhydrous upper-mantle minerals: concentration levels and implications. Eur J Mineral 12: 543–570

Ingrin J, Hercule S, Charton T (1995) Diffusion of hydrogen in diopside: results of dehydration experiments. J Geophys Res 100: 15489–15499

Ingrin J, Latrous K, Doukhan JC, Doukhan N (1989) Water in diopside: an electron microscopy and infrared spectroscopy study. Eur J Mineral 1: 327–341

Mackwell SJ, Kohlstedt DL (1990) Diffusion of hydrogen in olivine: implications for water in the mantle. J Geophys Res 95: 5079–5088

Libowitzky E, Rossman GR (1997) An IR absorption calibration for water in minerals. Am Mineral 82: 1111–1115

Rauch M, Keppler H (2002) Water solubility in orthopyroxene. Contrib Mineral Petrol 143: 525–536

Skogby H (1994) OH incorporation in synthetic clinopyroxene. Am Mineral 79: 240–249

Skogby H., Rossman GR (1989) OH- in pyroxene: an experimental study of incorporation mechanism and stability. Am Mineral 74: 1059–1069

Skogby H, Bell DR, Rossman GR (1990) Hydroxide in pyroxene: variations in the natural environment. Am Mineral 75: 764–774

Stalder R (2002) Synthesis of enstatite at high pressure. Eur J Mineral 14: 637–640

Wang L, Zhang Y, Essene E (1996) Diffusion of the hydrous component in pyrope. Am Mineral 81: 706–718